Autovetter Planet Candidate Catalog for Q1-Q17 Data Release 24

KSCI-19091-001
Joseph H. Catanzarite
20 July 2015

NASA Ames Research Center
Moffett Field, CA 94035

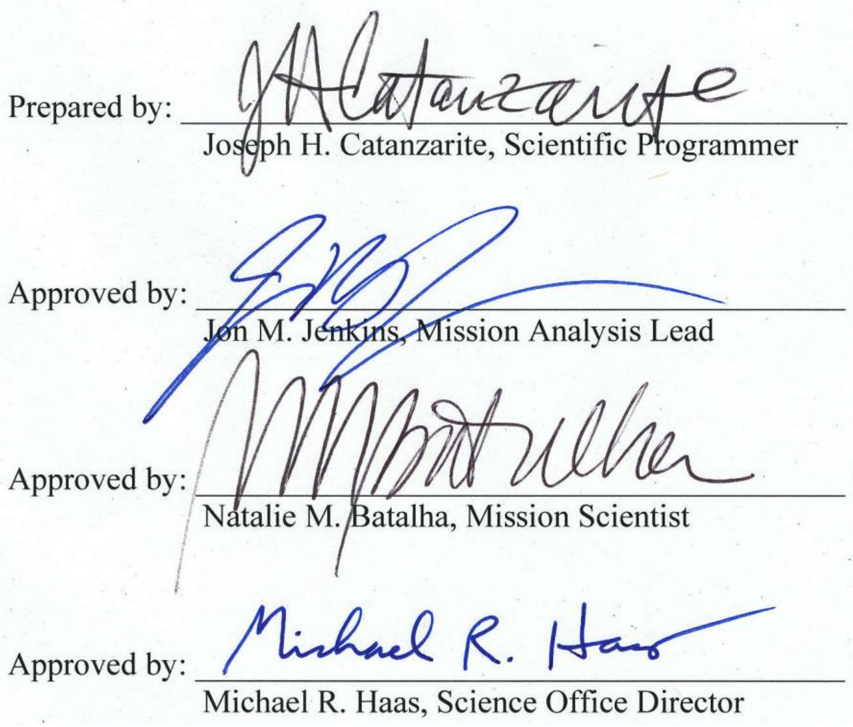

Prepared by: JHCatanzarite Date 7/20/15
Joseph H. Catanzarite, Scientific Programmer

Approved by: Date 7/20/15
Jon M. Jenkins, Mission Analysis Lead

Approved by: Date 7/20/15
Natalie M. Batalha, Mission Scientist

Approved by: Michael R. Haas Date 7/20/15
Michael R. Haas, Science Office Director

Approved by: Date 7/20/15
Steve B. Howell, Project Scientist

Document Control

Ownership

This document is part of the *Kepler* Project Documentation that is controlled by the *Kepler* Project Office, NASA/Ames Research Center, Moffett Field, California.

Control Level

This document will be controlled under KPO @ Ames Configuration Management system. Changes to this document **shall** be controlled.

Physical Location

The physical location of this document will be in the KPO @ Ames Data Center.

Distribution Requests

To be placed on the distribution list for additional revisions of this document, please address your request to the *Kepler* Science Office:

Michael R. Haas
Kepler Science Office Director
MS 244-30
NASA Ames Research Center
Moffett Field, CA 94035-1000

or

Michael.R.Haas@nasa.gov

DOCUMENT CHANGE LOG

CHANGE DATE	PAGES AFFECTED	CHANGES/NOTES
July 20, 2015	all	First issue

Table of Contents

1. Introduction

The ***autovetter*** is a machine learning based classifier that dispositions TCEs into three classes: PC (Planet Candidate), AFP (Astrophysical False Positive), and NTP (Non-Transiting Phenomenon), defined as follows:

- Class PC contains signals that are consistent with transiting planets, and for which no known reason exists to rule out that hypothesis.
- Class AFP contains signals of astrophysical origin that could mimic planetary transits, such as detached and contact eclipsing binaries, pulsating stars, starspots, and other periodic signals for which there is strong evidence to rule out a transiting planet origin.
- Class NTP contains signals that are evidently of instrumental origin, or are noise artifacts.

This document describes the autovetter, and how it is used to produce a catalog of Planet Candidates from the Q1-Q17 DR24 TCEs (Threshold Crossing Events) that are identified in the *Kepler* SOC (Science Operations Center) pipeline [Jenkins 2010ab] version 9.2 [Seader et al. 2015].

Classification is accomplished by means of a decision tree-based machine learning technique known as the ***random forest***. The inputs to the autovetter are a ***training data set*** composed of TCEs that have been dispositioned (mostly) by humans into these three classes, and a set of ***attributes*** (scalar statistics) associated with each TCE. From the training set, the autovetter 'learns' a mapping between attributes and predicted class. This mapping is then applied uniformly and consistently to all TCEs to produce a catalog of planet candidates.

1.1 Motivation for Another Planet Candidate Catalog

The *Kepler* project has produced the Q1-Q17 DR24 KOI (*Kepler* Object of Interest) activity table, which is hosted by NExScI (NASA Exoplanet Science Institute) and contains a catalog of planet candidates. This table was produced by the ***robovetter***, an expert system designed to automatically classify TCEs [Coughlin 2015], and will henceforth be referred to as the robovetter catalog.

The autovetter produces a different catalog of planet candidates. One might ask: why offer two catalogs? The autovetter and robovetter followed independent methodology to arrive at the same goal – automation of the process of human classification of planet candidates to achieve fast, robust and consistent vetting of the entire population of TCEs. The 'machine learning' approach differs from the 'expert system' approach in that the autovetter's decision rules are 'learned' autonomously from the data, while the robovetter operates with explicitly constructed decision rules.

The autovetter and robovetter evolved in parallel, learning from each other iteratively. The process has benefitted both, improving their respective planet catalogs. For example, early robovetter results indicated that the autovetter was initially misclassifying some TCEs with secondary eclipses as planet candidates; by adding new attributes we improved the autovetter's ability to correctly classify secondary eclipses. In the other direction, autovetter results showed that the robovetter was too strongly rejecting candidates based on diagnostics indicating a possible centroid offset, which allowed the robovetter to be tuned to mitigate that problem.

Though the two catalogs have converged over time, they don't always agree on classification for individual TCEs, nor would we expect them to, given the distinctly different origin of the decision rules for the autovetter and robovetter. As an example the autovetter tends to classify planets that are large enough and bright enough to have secondary eclipses as AFPs, while the robovetter is tuned to be able to identify them as PCs.

Another important difference is that while the autovetter has three classifications, PC/AFP/NTP, the robovetter has four flags: Not Transit-Like, Significant Secondary, Centroid Offset, and Ephemeris Match. These flags allow various sub-populations (e.g., on- and off-target EBs, off-target flux PCs, secondary eclipses) to be selected for further study.

The most important difference between the catalogs is that in addition to a predicted classification for each TCE, the autovetter also provides a Bayesian estimate of the ***posterior probability*** that the TCE is a member of each class. For a given TCE, the posterior probability for the class PC is a measure of the confidence that the TCE is a planet. Posterior probabilities can be advantageously used in statistical studies such as occurrence rate calculations to de-weight planet candidates that are at the noisy edges of the planet catalog.

Finally, we note that the autovetter results, which can be found in the Q1-Q17 DR24 TCE table at NExScI, change neither the dispositions in any KOI activity table nor the *Kepler* planet candidate count.

1.2 Overview of This Document

We describe the autovetter inputs and outputs in sections 2 and 3. In section 4, we provide some background on decision trees and the random forest. In section 5 we describe the attributes that are used by the random forest to classify TCEs. In section 6, we describe how the training set is constructed. In section 7 we describe the computation and use of posterior class probabilities. In Section 8 we present the autovetter catalog and give a detailed comparison of its results with those of the robovetter catalog. References are provided in Section 9.

2. Autovetter Inputs

The autovetter requires two inputs: the ***attributes matrix*** and the ***training data set***. Attributes are the scalar parameters and diagnostic statistics that are computed for each TCE. They include fitted transit parameters (such as period, transit depth, transit epoch), stellar parameters (such as effective temperature and gravity), as well as signal to noise and chi-squared from the transit model fits. The attributes matrix has a row for each TCE and a column for each attribute. A list of attribute names is provided in section 5.
The training data set consists of labels PC (planet candidate), AFP (astrophysical false positive), and NTP (non-transiting phenomenon) for a subset of several thousand TCEs. The PC labels in our training set are derived from dispositions originally produced via a manual vetting process developed by the TCERT (Threshold Crossing Event Review Team). The AFP and NTP labels come from TCERT dispositions combined with other diagnostics. For the purpose of training the autovetter, the training set labels are considered to be 'ground truth'. The construction of the training data set is discussed in detail in section 7.

3. Autovetter Outputs

The autovetter produces the following outputs for each TCE:

a) Random forest vote fraction, in percent, for each class (PC, AFP, NTP),
b) Uncertainty in random forest vote fraction, in percent, for each class,
c) Posterior class probabilities that the TCE is a member of each of the three classes,
d) An autovetter-determined classification (PC, AFP or NTP), and
e) A training label (PC, AFP, or NTP), if the TCE was in the training set.

Description of the autovetter outputs

av_vf_pc, av_vf_afp, av_vf_ntp (float)
Vote fraction value for classes PC, AFP and NTP, respectively (float, in percent). For each class, the vote fraction value is the mean class vote fraction for a set of 10 random forest runs.

av_vf_pc_err, av_vf_afp_err, av_vf_ntp_err (float)
Uncertainty in the vote fraction for classes PC, AFP and NTP, respectively (float, in percent). For each class, the error in the mean class vote fraction from a set of 10 random forest runs is the standard deviation in the class vote fraction divided by the square root of 10.

av_pp_pc, av_pp_afp, av_pp_ntp (float)
Posterior class probabilities for PC, AFP and NTP classifications, respectively (float, in percent).

av_pred_class (char)
Classifications predicted by the autovetter, which are the optimum MAP (maximum a posteriori) classifications. Values are ‘PC’, ‘AFP’, or ‘NTP’.

av_training_set (char)
Training labels: if the TCE was included in the training set, the training label encodes what we believe is the ‘true’ classification, and takes a value of either ‘PC’, ‘AFP’, or ‘NTP’. Training labels are given a value of ‘UNK’ for TCEs that are not included in the training set.

For details about the determination of posterior probabilities and optimum MAP classifications see [Jenkins 2015c].

4. Decision Trees and the Random Forest

A ***decision tree*** is a hierarchical series of one-dimensional inequalities that partitions the phase space of ***attributes***. At each split, a hyperplane divides a single attribute into a left branch and a right branch, in which the attribute's value is less than (left branch) or greater than (right branch) the value at the split.

A split reduces entropy when it partitions the data into regions in which the class populations are more sharply differentiated than they were before the split. Which attribute to split on and the value of that attribute at the split are chosen to maximize the resulting entropy reduction. Successive splits are carried out according to this entropy-reduction principle. Each split produces two new branches in the tree. Splitting continues until no further entropy-reducing splits are available. The terminal split on each branch produces a pair of ***leaf nodes***, regions of phase space in which the class populations should be highly differentiated to favor one class. The full set of splits defines the decision tree classifier, which maps any vector in attributes phase space to the predicted classification associated with the leaf node in which the vector lies.

The random forest refines the decision tree approach in two ways. The first refinement is called ***bootstrap*** aggregation or ***bagging***. Instead of a single tree, a 'forest' of trees is generated from a set of bootstrap samples of the training data set (also called a ***bag***). A bootstrap sample is an ensemble of examples drawn with replacement from the training set, and of the same size as the training set. On average, a bootstrap sample uses about 2/3 of the training set. The remaining 1/3 of the training set are called ***out-of-bag*** samples. Because they are not used in that decision tree, they are available to estimate classification error without committing the crime of 'data snooping'. For this reason, the random forest does not require cross-validation to estimate classification error. Bagging decreases the variance of the classifier, meaning that it reduces its sensitivity to the characteristics of a particular training set, thus mitigating the problem of ***overfitting***. The second refinement is that at every split, the attribute to split on is chosen from a different small random subset of the attributes, instead of from the entire set of attributes. If the splitting attribute were always selected from the entire set of attributes, the trees will tend to look similar, since the strongest attribute will be chosen at each split. Choosing the splits from small random samples of attributes effectively ***decorrelates*** the trees. For each example, the predicted class is then decided by the majority vote among all the trees in the random forest.

The two parameters that control the random forest are the number of trees in the forest and the size of the random subset of attributes to choose from at each split. The number of trees can be optimized by incrementally increasing it until there is no improvement in the classification error. We find that good results can be obtained with forests of 10,000 trees. Following standard practice, we took the size of the random subset of attributes that is used at each split to be the square root of the number of attributes.

For more details about the random forest, see [Breiman 2001] and [James 2013]. Implementation of the random forest in the autovetter is discussed in [McCauliff 2015] and [Jenkins 2015c].

5. The Attributes Matrix

Attributes are scalar quantities that are computed for each TCE. Ideally, attributes capture characteristics that aid in classification. Unlike classification methods that depend upon distances between points in attribute phase space, the random forest is robust to missing attribute values; not all attributes need exist for each example. Because each split must be chosen from a small random subset of the attributes, the random forest is relatively robust to correlations in the attributes.

An attribute's ***importance*** is measured by the increase in the overall classification error rate that would result from randomly scrambling the values of that attribute among all the out-of-bag examples. Table 1 lists 114 attributes that the autovetter used, sorted in order of importance. Attributes whose importance fell below an empirically determined importance threshold of 5×10^{-5} were not used and are not listed. Sorted importances for the 114 attributes are plotted in Figure 1.

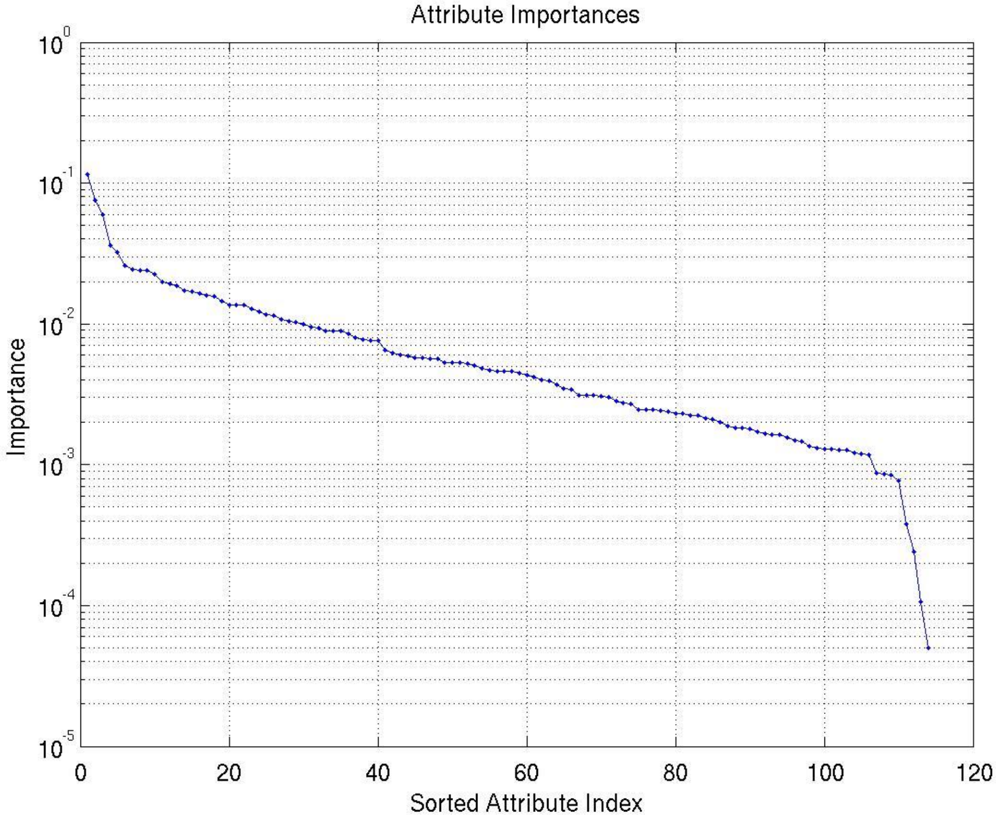

Figure 1. Sorted importances for the 114 attributes used by the autovetter.

It is beyond the scope of this document to provide complete descriptions of all the attributes in Table 1. That said, many of the attribute names are self-descriptive. Most of the attributes are computed in the DV (Data Validation) section of the *Kepler* SOC pipeline [Wu 2010]. It is possible, however, to formulate and compute new attributes post hoc, after the pipeline has completed. We have done this in several cases, which we will discuss in the next section, where we will identify and describe a few of the most important attributes and indicate how they are computed. For brief descriptions of more of the important attributes, see [Jenkins 2015c].

Table 1. Attributes Used by the Autovetter and Their Importances

1. minLongerShorterPeriodSignificance
2. lppStatistic
3. numberOfPlanets
4. planetCandidate.weakSecondaryStruct.maxMes
5. planetCandidate.weakSecondaryStruct.mesMad
6. binaryDiscriminationResults.longerPeriodComparisonStatistic.significance
7. binaryDiscriminationResults.shorterPeriodComparisonStatistic.significance
8. binaryDiscriminationResults.longerPeriodComparisonStatistic.value
9. binaryDiscriminationResults.shorterPeriodComparisonStatistic.value
10. chiSquareGof
11. bootstrap_falseAlarmRate
12. evenTransitsFit_ratioSemiMajorAxisToStarRadius_value
13. oddTransitsFit_ratioSemiMajorAxisToStarRadius_value
14. maxEphemerisCorrelationAllStars
15. minMesMaxMesRatio
16. centroidResults.differenceImageMotionResults.mqKicCentroidOffsets.meanSkyOffset.value
17. edgeStat
18. allTransitsFit_ratioSemiMajorAxisToStarRadius_value
19. centroidResults.differenceImageMotionResults.mqKicCentroidOffsets.meanSkyOffset.significance
20. sesProbability
21. tEquilibrium
22. tBrightness
23. centroidResults.fluxWeightedMotionResults.motionDetectionStatistic.significance
24. allTransitsFit.modelFitSnr
25. allTransitsFit.modelChiSquare
26. centroidResults.fluxWeightedMotionResults.motionDetectionStatistic.value
27. allTransitsFit_orbitalPeriodDays_value
28. planetCandidate.modelChiSquare2
29. numSesInMes
30. evenTransitsFit_orbitalPeriodDays_value
31. centroidResults.differenceImageMotionResults.summaryQualityMetric.fractionOfGoodMetrics
32. oddTransitsFit_ratioSemiMajorAxisToStarRadius_uncertainty
33. evenTransitsFit_ratioSemiMajorAxisToStarRadius_uncertainty
34. evenTransitsFit.modelChiSquare
35. evenTransitsFit.modelFitSnr
36. modelFitSnrToMesRatio
37. centroidResults.differenceImageMotionResults.mqControlCentroidOffsets.meanSkyOffset.value
38. allTransitsFit_planetRadiusEarthRadii_value
39. centroidResults.fluxWeightedMotionResults.sourceOffsetArcSec.value
40. allTransitsFit_ratioSemiMajorAxisToStarRadius_uncertainty
41. effectiveTemp.value
42. centroidResults.differenceImageMotionResults.mqKicCentroidOffsets.meanSkyOffset.uncertainty
43. oddTransitsFit.modelChiSquare.reducedchi
44. oddTransitsFit_planetRadiusEarthRadii_value
45. evenTransitsFit_semiMajorAxisAu_value
46. centroidResults.differenceImageMotionResults.mqControlCentroidOffsets.meanSkyOffset.uncertainty
47. chiSquare7
48. evenTransitsFit_planetRadiusEarthRadii_value
49. allTransitsFit_semiMajorAxisAu_uncertainty

50. chiSquare1
51. allTransitsFit_ratioPlanetRadiusToStarRadius_value
52. oddTransitsFit_ratioPlanetRadiusToStarRadius_value
53. allTransitsFit_orbitalPeriodDays_uncertainty
54. radius.value
55. oddTransitsFit_transitDepthPpm_value
56. allTransitsFit_transitDurationHours_uncertainty
57. allTransitsFit_transitIngressTimeHours_value
58. maxEphemerisCorrelationSameStar
59. reducedParameterFits_1.modelChiSquare.delta
60. nPulsesFlaggedAsPlanet
61. evenTransitsFit_transitDepthPpm_value
62. depthStat
63. allTransitsFit_transitDepthPpm_value
64. centroidResults.fluxWeightedMotionResults.sourceOffsetArcSec.uncertainty
65. oddTransitsFit_transitIngressTimeHours_value
66. evenTransitsFit_inclinationDegrees_value
67. binaryDiscriminationResults.oddEvenTransitDepthComparisonStatistic.significance
68. evenTransitsFit_transitIngressTimeHours_value
69. tBrightnessUpperFractionalErrorBar
70. albedo
71. evenTransitsFit_transitDurationHours_value
72. evenTransitsFit_semiMajorAxisAu_uncertainty
73. epochKjd
74. allTransitsFit_inclinationDegrees_value
75. robustStatisticToMesRatio
76. evenTransitsFit_minImpactParameter_uncertainty
77. evenTransitsFit_transitDurationHours_uncertainty
78. allTransitsFit_transitDurationHours_value
79. oddTransitsFit_transitDurationHours_value
80. evenTransitsFit_transitEpochBkjd_uncertainty
81. tBrightnessLowerFractionalErrorBar
82. evenTransitsFit_transitIngressTimeHours_uncertainty
83. keplerMag
84. evenTransitsFit_ratioPlanetRadiusToStarRadius_uncertainty
85. oddTransitsFit_transitEpochBkjd_uncertainty
86. rmsCdpp
87. allTransitsFit_planetRadiusEarthRadii_uncertainty
88. allTransitsFit_transitDepthPpm_uncertainty
89. chiSquareDof10
90. evenTransitsFit_planetRadiusEarthRadii_uncertainty
91. tEquilibriumLowerFractionalErrorBar
92. oddTransitsFit_inclinationDegrees_uncertainty
93. evenTransitsFit_transitDepthPpm_uncertainty
94. cdppSlope
95. normCompSum
96. allTransitsFit_inclinationDegrees_uncertainty
97. binaryDiscriminationResults.oddEvenTransitDepthComparisonStatistic.value
98. allTransitsFit_transitIngressTimeHours_uncertainty
99. mesGrowthStat
100. evenTransitsFit_inclinationDegrees_uncertainty
101. allTransitsFit_minImpactParameter_uncertainty
102. oddTransitsFit_minImpactParameter_value
103. allTransitsFit_ratioPlanetRadiusToStarRadius_uncertainty
104. planetCandidate.weakSecondaryStruct.maxMesPhaseInDays
105. skyGroupId
106. albedoUpperFractionalErrorBar

107. allTransitsFit_minImpactParameter_value
108. binaryDiscriminationResults.oddEvenTransitEpochComparisonStatistic.value
109. planetCandidate.weakSecondaryStruct.minMesPhaseInDays
110. diffRatioSemiMajorAxisToStarRadiusV
111. planetCandidate.weakSecondaryStruct.maxMesPhaseInDays.normalized
112. detectedFeatureCount
113. removedFeatureCount
114. planetCandidate.suspectedEclipsingBinary

6. Building the Training Set

All supervised machine-learning classifiers require a ***training set*** of ***examples*** with known ***class labels***. In this application, the examples are TCEs; there are three classes with labels PC, AFP, and NTP. In this section, we describe the construction of the training set that was used to produce the autovetter catalog. The training set contains 3600 PCs, 9596 AFPs and 2541 NTPs, and is available at NExScI as part of the Q1-Q17 DR24 TCE table.

The training set and its attributes are ultimately used to build a ***random forest classifier*** that maps the attributes of any TCE to a predicted class label of either PC, AFP, or NTP. It is important to have representative examples of each class that span the entire range of expected characteristics. It is also important to develop and include attributes that can help identify features characteristic of each of the different classes. In this section we will see both aspects of this strategy in action.

The autovetter class definitions differ somewhat from those used by the robovetter to create the KOI (*Kepler* Object of Interest) catalogs [Batalha 2013], [Borucki 2011a], [Borucki 2011b], [Burke 2014], [Coughlin 2015], [Mullally 2015], and [Rowe 2015]. The robovetter identifies TCEs whose light curves lack a transit signature characteristic of a planet or a non-contact eclipsing binary with a Not Transit Like flag. This can include TCEs with periodic light curve variations due to contact binaries, starspots, and pulsations. The remaining TCEs are christened as KOIs, which are then dispositioned as either PC (planet candidates), or FP (False Positives). The robovetter PC class is almost the same as that of the autovetter, the only difference being that the autovetter defines a PC to have radius smaller than 25 R_{Earth} in the training set. The FP class contains predominantly TCEs that have transit-like signals consistent with a transiting planetary or (non-contacting) stellar companion. The robovetter FP class is a subset of the autovetter AFP class, in which we have chosen to also include TCEs produced by periodic signals of astrophysical origin that are due to pulsating stars, contact binaries and starspots; the robovetter would classify these as Not Transit-Like.

6.1 Training Examples from TCERT

The first step is to include a large number of examples of planet candidates and false positives, as determined by the TCERT. These came from the cumulative KOI (*Kepler* Object of Interest) activity table, downloaded on 13 Feb 2015 from the NExScI archive after the Q1-Q12 and Q1-Q16 tables were closed as ‘done’. We match the transit ***ephemerides*** (transit epoch, period, and duration) of the KOIs from the cumulative KOI table to those of the Q1-Q17 TCEs. We label the TCERT planet candidates as PC, and the false positives as AFP in the training set.

TCERT does not use planet radius to determine whether a TCE should be made a PC. But the largest known exoplanet is HAT-P-32b with radius of 22.5 Earth radii. If a transiting object has a radius larger than 25 Earth radii, it is likely to be a star rather than a planet. We therefore apply a planet radius cut, changing the labels of 135 PC (planet candidate) KOIs with radii exceeding 25 R_{Earth} to AFP (astrophysical false positive).

6.2 Multiple TCEs at the Same Period on a Target

Often, the secondary of an eclipsing binary or a residual signal from a primary transit will generate one or more TCE(s) with similar characteristics. Other cases of astrophysical origin that might generate multiple TCEs at the same period on a target star include contact binaries, starspots, and pulsations. To identify this type of TCE, we calculate a statistic called **minLongerShorterPeriodSignficance** that tests whether the TCE's period is close to that of another TCE on the same target star, and add it to the attributes matrix. It turns out that **minLongerShorterPeriodSignficance** is ranked as the most important attribute (see Table 1). Another way to identify this type of TCE is to calculate the Pearson's correlation coefficient between its ephemeris and the ephemerides of each of the other TCEs on the same star. For each TCE, we calculate the maximum of these correlation coefficients, **maxEphemerisCorrelationSameStar** and add this to the attributes matrix. If the TCE's ephemeris is highly correlated with that of another TCE on the same star, it is most likely due to a residual of another TCE. The attribute **maxEphemerisCorrelationSameStar** is ranked #58 in importance (see Table 1). By including in the training set a sufficient number of examples of TCEs with periods close to those of other TCEs on the same target (these are common among the TCERT false positives), we trained the autovetter to classify similar TCEs as AFPs.

6.3 Contaminated TCEs

It is possible for a bright star with a periodic signal (such as an eclipsing binary or an RR Lyrae variable) to contaminate – i.e. imprint its periodic signature on – other targets on the focal plane. Flux from the PRF (Point Response Function) of a bright star, or flux from an ***optical ghost*** can overlap the PRF of a target star. Optical ghosts are caused by reflections from the CCD surface to the field-flattening lenses (or the Schmidt corrector lens) and back to the CCD. The reflection creates an out-of-focus image of the source star. Flux from an optical ghost can contaminate stars many pixels away from a bright source on the focal plane. For a detailed study of this phenomenon, see [Coughlin 2014].

We found 1437 TCEs that were ephemeris-matched to eclipsing-binary contaminators; these were labeled as AFP and added to the training set if they were not already included among the TCERT false positives.

Another class of contaminated TCEs has a spurious 459-day period, which has been identified as an instrumental systematic; 265 TCEs whose light curves show this signature were identified. Since these signals are not astrophysical in origin, we labeled them as NTP and included them (if they were not already present) in the training set.

210 TCEs were found to be ephemeris-matched to an RR Lyrae contaminator and were also labeled as NTP and included in the training set. However, to be consistent with our classification scheme we should have labeled them as AFP (since their periodicity is astrophysical in origin). We believe that changing the labels of these TCEs to AFP in future training sets might lead to improvement in the autovetter's ability to separate the AFP and NTP classes.

A TCE that shows a high correlation with a TCE on another target is most likely to be contaminated by mechanisms such as the ones discussed above. In order to improve the autovetter's sensitivity to contamination, we computed a statistic called **maxEphemerisCorrelationAllStars**, which is the maximum of the Pearson's correlation coefficient of each TCE's ephemeris with the ephemerides of all TCEs on other stars. We appended this column vector to the attributes matrix. Of all the attributes, **maxEphemerisCorrelationAllStars** ranks #14 in importance (see Table 1).

6.4 Other types of TCEs that correspond to Non-Transiting Phenomena (NTP)

The LPP (locality preserving projection) statistic has been shown to provide excellent separation between light curves with and without a transit signal, so it should effectively distinguish NTPs from AFPs and PCs. We included the LPP statistic as a column in the attributes matrix, so that the autovetter could learn to make use of it. It is ranked at #2 in attribute importance (see Table 1). The LPP statistic is presented in [Thompson 2015].

Another tool for identifying TCEs of class NTP is the ***bootstrap test***, which identifies TCEs whose false alarm probability exceeds some threshold, making them highly likely to be statistical false alarms. We use the newest, corrected version of the bootstrap (developed for the 9.3 pipeline release) and applied a false alarm probability threshold of 10^{-11}. TCEs that failed the bootstrap test at a threshold of 10^{-11} were labeled as NTP and included in the training set. For a discussion of the bootstrap, see [Jenkins 2015a] and [Seader 2015], as well as the Appendix of [Jenkins 2015b].

In the Q1-Q12 catalog generation process, a large number of TCEs were visually inspected by the TCERT team and classified as 'not KOIs'. We ephemeris-matched 1790 of these TCEs to the Q1-Q17 TCEs. We labeled as NTP and included in the training set any of these that were not already included in the training set as AFPs.

Sometimes a TCE is produced by an event that is not physically consistent with a transit. The MES ratios test computes ratios of the **robustStatistic** and **modelFitSnr** to the **maxMES** (maximum multiple-event statistic). These three attributes are provided by the DV (data validation) component of the *Kepler* pipeline. A low ratio of **robustStatistic** or **modelFitSnr** to the **maxMES** indicates that the transits are of inconsistent depth, or that the transit pulse is not well matched to a physically realistic transit waveform. We found 171 TCEs for which both ratios were less than 0.5; these were labeled as NTP and included in the training set. We note that no PCs from the NExScI catalog failed the MES ratios test. We included both the ratio of the **robustStatistic** to the **maxMES** and the ratio of the **modelFitSnr** to the **maxMES** in the attributes matrix so that the autovetter can learn to make use of them. These ratios rank at #75 and #36, respectively, in attribute importance (see Table 1). The MES ratios test is discussed in more detail in [Jenkins 2015c].

Another class of objects that we label as NTP in the training set are KOIs from the NExScI cumulative table that had the 'not-transit-like' flag set to true, and had both ‘significant secondary’ flag and ‘centroid offset’ flags set to false, because the NTP class should logically include these.

6.5 Bad TCEs

Finally, there were 74 TCEs that were determined by TCERT to be ‘bad TCEs’ because their detections were triggered by residuals of fitted transits; these were excluded from the training set.

7. Posterior Class Probabilities

The output of the random forest classifier depends on the ***prior class probabilities*** of the training data set. If these are different than those of the TCEs we want to classify, then the classification accuracy may be sub-optimal. For example, if the data to be classified has a greater proportion of NTPs than the training set, a classifier that is more biased toward NTPs could have a lower classification error than the current random forest. We can correct for such biases by re-weighting the vote fractions so that NTP is chosen at a lower vote threshold. Starting with initial estimates for the priors for the class probabilities of PC, AFP, and NTP, it is possible to re-weight the random forest vote fractions so as to minimize the total number of misclassifications across the training set and estimate the prior class probabilities of the whole TCE population. An iterative bootstrap approach to accomplish this optimization is outlined in [Jenkins 2015c].

With knowledge of prior class probabilities one can proceed to estimate posterior class probabilities via Bayes' Rule. Posterior class probabilities reflect our confidence that the TCE belongs to the predicted class; they are an internal measure of the reliability of the classification.

Figures 3 and 4 display the autovetter classification results in the form of a ***ternary diagram*** (Cf. section 8). Vertices of the ternary diagram correspond to each of the three classes; at a vertex there is a probability of one to be in the associated class, and a probability of zero to be in any other class. We would expect to have high confidence in the predicted class of a TCE if it is near a vertex and much lower confidence if it is near a decision boundary (the lines separating the colored regions). How this intuition can be quantified to give posterior class probabilities for every TCE is shown in [Jenkins 2015c]. The key is the development of a non-Euclidean distance metric in the phase space of the ternary diagram, leading to estimates of class posterior probability densities as a function of the reweighted class votes. With a method to compute posterior probabilities in hand, a naive Bayes classifier is overlaid on the random forest vote fractions, and the MAP (maximum a posteriori probability) that gives optimal agreement with the random forest is determined.

Posterior class probabilities lead to an important refinement of occurrence rate calculations. Instead of giving equal weight to each PC detection, it is possible to count each PC detection as a 'fractional planet' with the fraction equal to the PC posterior probability, ranging from zero to one. In this scheme, planet candidates with low posterior probabilities naturally influence the occurrence rate less than those with high posterior probabilities. Planet candidates in the critical regimes of low SNR, long period, and small radius are counted but prevented from severely skewing the occurrence rate, as would happen if each detection was counted as one planet.

The foregoing discussion naturally leads to a further possibility: abandon votes and classifications altogether, and instead count *every* TCE (as a fraction of a planet equal to its PC posterior probability) in the occurrence rate. For example, suppose a TCE is near a decision boundary (see Figure 3), with 50% AFP posterior probability, 40% PC posterior probability, and 10% NTP probability, and is classified as AFP by the optimal weighted votes. This TCE would therefore contribute 40% of a detected planet in an occurrence rate calculation. Extending this approach to include TCEs near the decision boundaries might be worthwhile, but including all non-PC TCEs no matter how small the posterior PC probability could significantly skew the results of an occurrence calculation.

8. Autovetter Results for the Q1-Q17 DR24 TCEs

In this section we present a statistical analysis of the autovetter predicted classifications of both the training set TCEs and the TCEs of UNKNOWN class. Then we turn to a comparison of the performance of the autovetter vs. the classifications derived from the ***robovetter*** [Coughlin 2015].

8.1 Performance of the Autovetter on the Training Set

The results of applying the autovetter classifier to the training set are expressed in terms of a ***confusion matrix*** in Table 2. Rows 1, 2, and 3 correspond to true class PC, AFP, and NTP. Columns 1, 2, and 3 correspond to predicted class PC, AFP, and NTP. For example, in column 1 we see that 107 AFP examples and 5 NTP examples were incorrectly classified as PC. In row 3 we see that of 2541 (5 + 77 + 2459) TCEs that are members of the NTP class, 5 were misclassified as PC and 77 were misclassified as AFP. The diagonal elements show the number of each class that were correctly classified, and the off-diagonal elements show the misclassifications. For example, the (3,3) element shows that 2459 TCEs were correctly classified as NTP; the (3,1) element shows that 5 TCEs that were labeled as members of the class NTP in the training set were incorrectly predicted to be members of the class PC.

Table 2. Autovetter Confusion Matrix

	Predicted class PC	Predicted class AFP	Predicted class NTP
True class PC	3495	96	9
True class AFP	107	9365	124
True class NTP	5	77	2459

The ***confusion rate matrix*** in Table 3 is derived from the confusion matrix by normalizing each row by the total number of elements in the corresponding true class.

Table 3. Autovetter Confusion Rate Matrix

	Predicted class PC	Predicted class AFP	Predicted class NTP
True class PC	0.971	0.027	0.002
True class AFP	0.011	0.976	0.013
True class NTP	0.002	0.030	0.968

From the confusion rate matrix, we compute the classification error rates, shown in Table 4. The overall error rate is the percentage of the training examples that were incorrectly classified. The PC, AFP and NTP error rates are the percentages of PC, AFP and NTP training examples that were incorrectly classified. Because the error rates were obtained using ‘out-of-bag’ samples, they also predict the ‘generalization error’, which is the performance that we expect when the autovetter classifier is applied to an ensemble of TCEs of UNKNOWN class. No cross-validation is necessary. The foregoing is true as long as the training set contains a representative sample of TCEs of UNKNOWN class.

The PC false alarm rate is the percentage of training examples that were incorrectly classified as PC; if the UNKNOWN TCEs have class frequencies that are the same as those of the training set, then we'd expect the same PC false alarm rate when the classifier is applied to the UNKNOWN TCEs.

Table 4. Autovetter Error Rates

Overall error rate	2.7 %
PC error rate	2.9 %
AFP error rate	2.4 %
NTP error rate	3.2 %
PC false alarm error rate	3.1 %

8.2 Classifying the Unknown TCEs

Figure 2 shows the autovetter catalog of 3900 planet candidates represented in planet radius vs. orbital period phase space. There were a total of 20367 TCEs, of which 15737 were in the training set and 4630 were of UNKNOWN class. From the training set, the autovetter classified 3495 of the PCs and 112 of the AFPs and NTPs as planet candidates (see Table 2). 293 of the UNKNOWN TCEs were also classified as planet candidates.

Since the PCs in the training set are from past search activities and generally represent the 'low-hanging' fruit, we expect that on average they should have higher SNR and larger radii than the PCs found among the UNKNOWN TCEs. Indeed, we find that the median radius and maximum MES (a proxy for SNR) are 2.0 Rearth and 22.1 for the training set PCs, compared to 1.2 Rearth and 8.7 for the 293 newly classified PCs.

If a planet candidate can be validated by external means such as radial velocity detection, or internal means (transit timing variations) it is given the NExScI classification of CONFIRMED. It is of interest to check how the autovetter classified these. We find that of the 972 TCEs classified as CONFIRMED, the autovetter classified 957 (98.46%) as PC, 14 (1.44%) as AFP, and 1 (0.10%) as NTP.

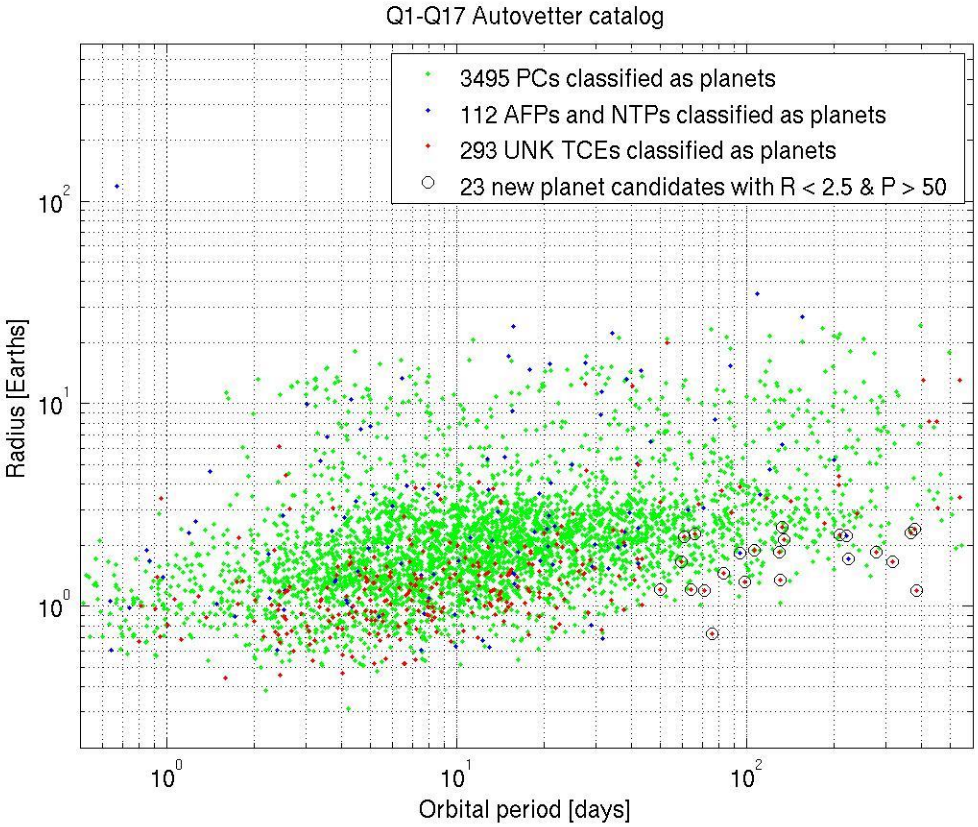

Figure 2. The autovetter catalog of 3900 planet candidates. Green points are TCEs that are PCs in the training set; blue points are AFPs and NTPs in the training set. Red points are TCEs that were not in the training set but were classified as PCs. Open black rings surround points of PCs with radius smaller than 2.5 Rearth and period longer than 50 days, a range that is of great interest in the calculation of planetary occurrence rates.

Figures 3 and 4 show ***ternary diagrams*** for the TCEs in the training set and TCEs of previously unknown class. Since the PC, AFP and NTP vote fractions add to one, only two are independent; we have chosen to display the NTP vote fraction along the abscissa and the PC vote fraction along the ordinate axis. Perfect PC candidates would be at the top right corner, perfect AFP candidates at the lower right corner, and perfect NTP candidates at the lower left corner. The densities are generally concentrated toward the corners of the triangle, and away from the decision boundaries (lines separating the colored regions), which is the hallmark of a good classifier. Classifications are the least certain for points that are near or on the decision boundaries.

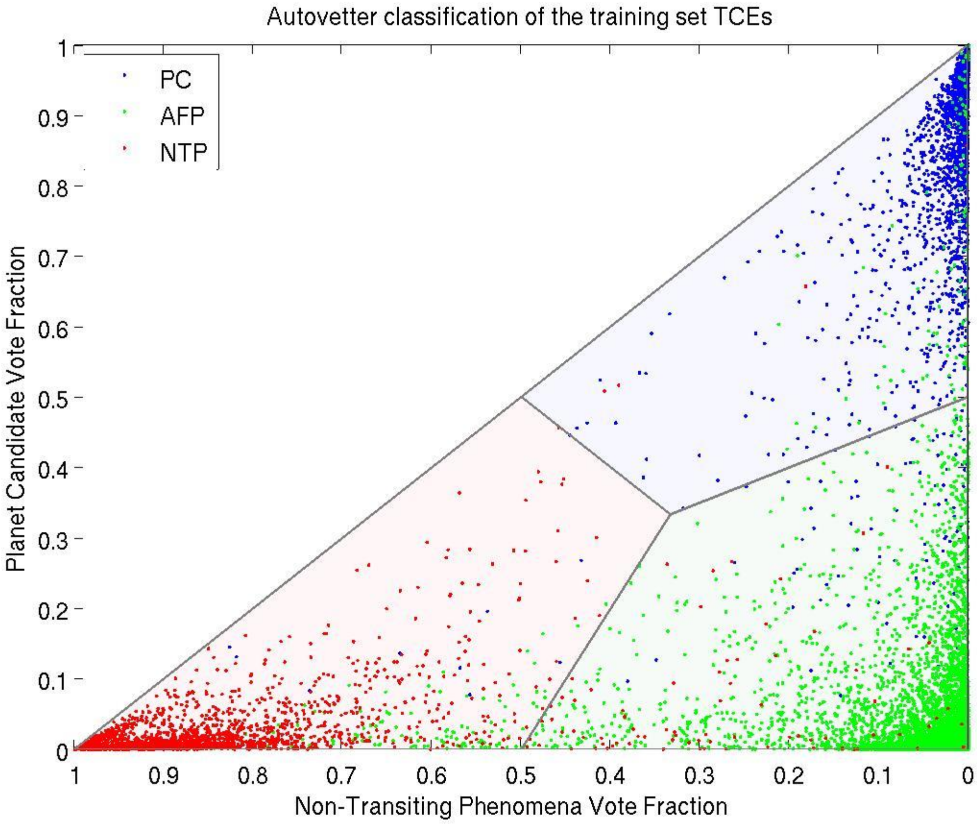

Figure 3. Autovetter classification of TCEs in the training set. Note that the densities are concentrated near the corners and away from the decision boundaries (the lines separating the three colored regions – blue for PC, green for AFP, and red for NTP). Separation of the three classes is observed to be quite good overall. There is some overlap between AFP and NTP and between AFP and PC; but NTP is well separated from PC. Classifications are the least certain for points that are near or on the decision boundaries.

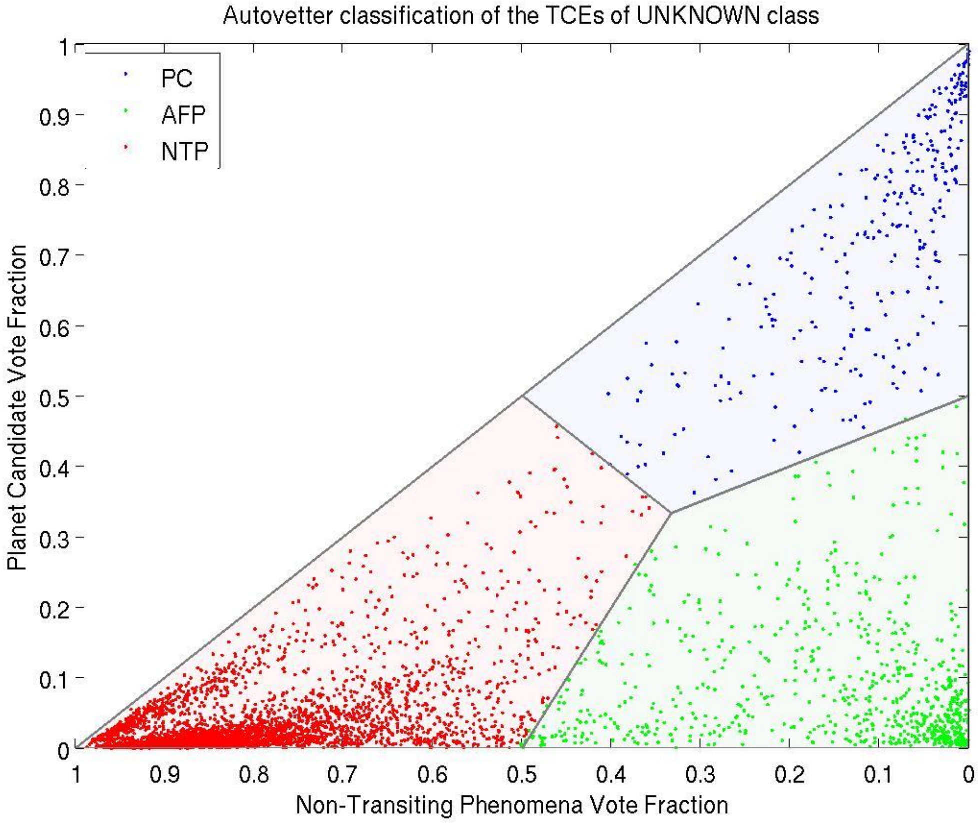

Figure 4. Autovetter classification of TCEs of UNKNOWN class. Again, the densities are concentrated near the corners of the triangle and away from the decision boundaries. Classifications are the least certain for points that are near or on the decision boundaries.

Histograms of posterior probability to be in the PC class are shown in Figures 5, 6, and 7 for TCEs that are classified as PC, AFP and NTP, respectively. Evidently, a TCE is overwhelmingly likely to be a PC if classified as a PC, and overwhelmingly unlikely to be a PC if not classified as a PC.

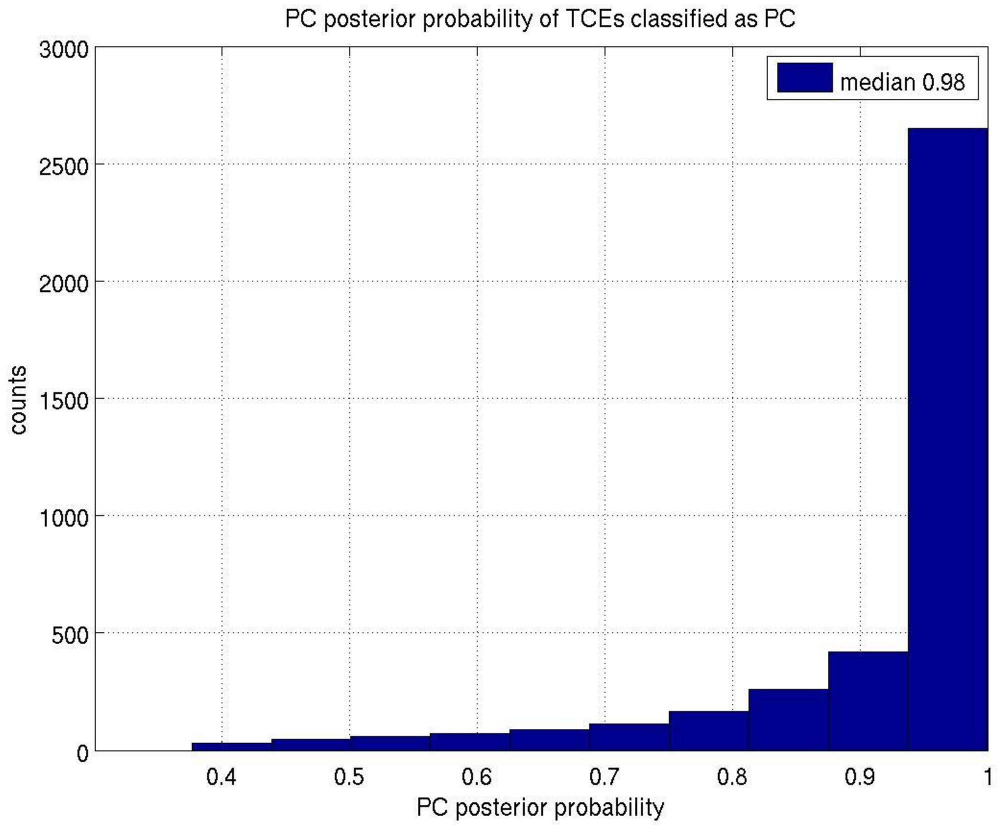

Figure 5. PC posterior probability for TCEs classified as PC. Most probabilities are quite close to 1, though a narrow tail extends downward.

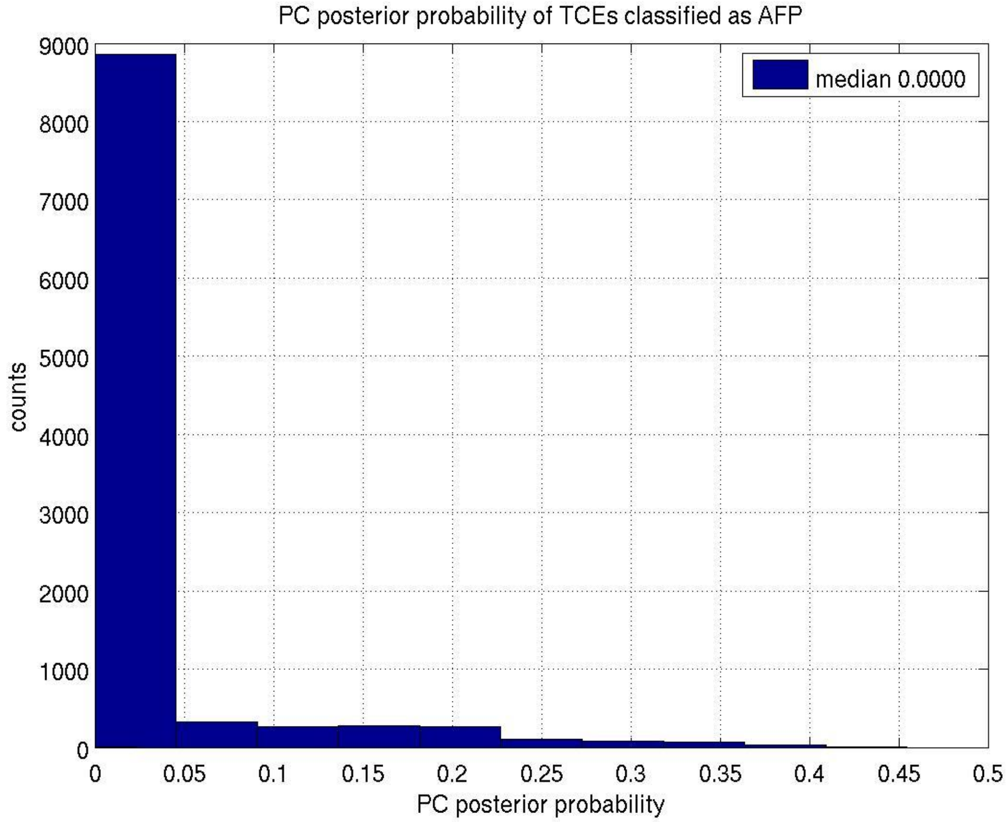

Figure 6. PC posterior probability for TCEs classified as AFP. The probabilities are concentrated near zero, though a narrow tail extends upward.

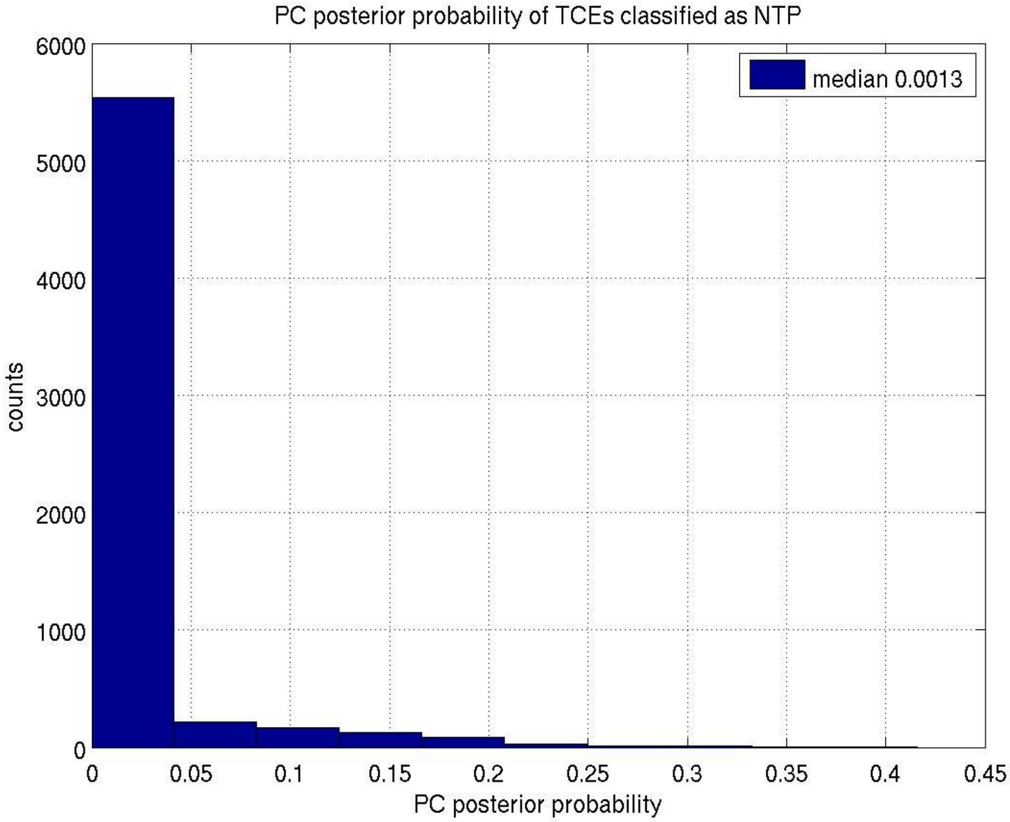

Figure 7. PC posterior probability for TCEs classified as NTP. The probabilities are concentrated near zero, though a narrow tail extends upward.

8.3 Comparison of the Autovetter Catalog to the Robovetter Catalog

The ***robovetter*** is an expert system designed to automatically classify TCEs based on heuristics developed by the TCERT team (see [Coughlin 2015]). The robovetter differs from the autovetter in that its heuristics are (with the exception of the Locality Preserving Projection) ‘hardwired’ by humans rather than ‘learned’ autonomously from the data. The robovetter first decides if a TCE is Not Transit Like; these TCEs are excluded from further consideration. The rest become KOIs, and are classified as either PC (planet candidate), or FP (false positive). FPs are KOIs with transit-like signatures that analysis has shown to be due to a star rather than a planet. Classifications by the robovetter have been delivered to NExScI and can be found in the Q1-Q17 DR24 KOI table. In this section we compare the autovetter catalog classifications against those of the robovetter catalog.

8.3.1 Overall TCE Classifications

The full comparison for the 7479 KOIs is given in Table 5. When the autovetter classifies a TCE as PC, the robovetter agrees 97.2% of the time. When the robovetter classifies a

TCE as PC, the autovetter agrees 87.9% of the time. From Table 5, we see that 10% of robovetter PCs are autovetter AFPs and 2.1% of robovetter PCs are autovetter NTPs.

Table 5. Comparison of Autovetter vs. Robovetter Classifications of KOIs (percentages add to 100% across rows)

Classification of 7479 KOIs	Robovetter class PC (4295)	Robovetter class FP (3184)
Autovetter class PC (3882)	3775 (97.2%)	107 (2.8%)
Autovetter class AFP (3251)	428 (13.2%)	2823 (86.8%)
Autovetter class NTP (346)	92 (26.6%)	254 (73.4%)

Of the remaining 12888 non-KOI TCEs, the autovetter classifies 18 (0.1%) as PC, 7013 (54.4%) as AFP, and 5857 (45.4%) as NTP.

8.3.2 Relation to Occurrence Rate Calculation

The calculation of occurrence rates is particularly sensitive to incompleteness in the planet catalog, which is most severe at long orbital periods and small planet radii [Burke 2015]. An interesting regime in planet radius and orbital period phase space for planet occurrence rate calculations is $R_{planet} < 5\ R_{Earth}$ and $P > 50$ days. The autovetter and robovetter find 429 and 449 planet candidates in this regime, respectively; these are shown in Figure 8.

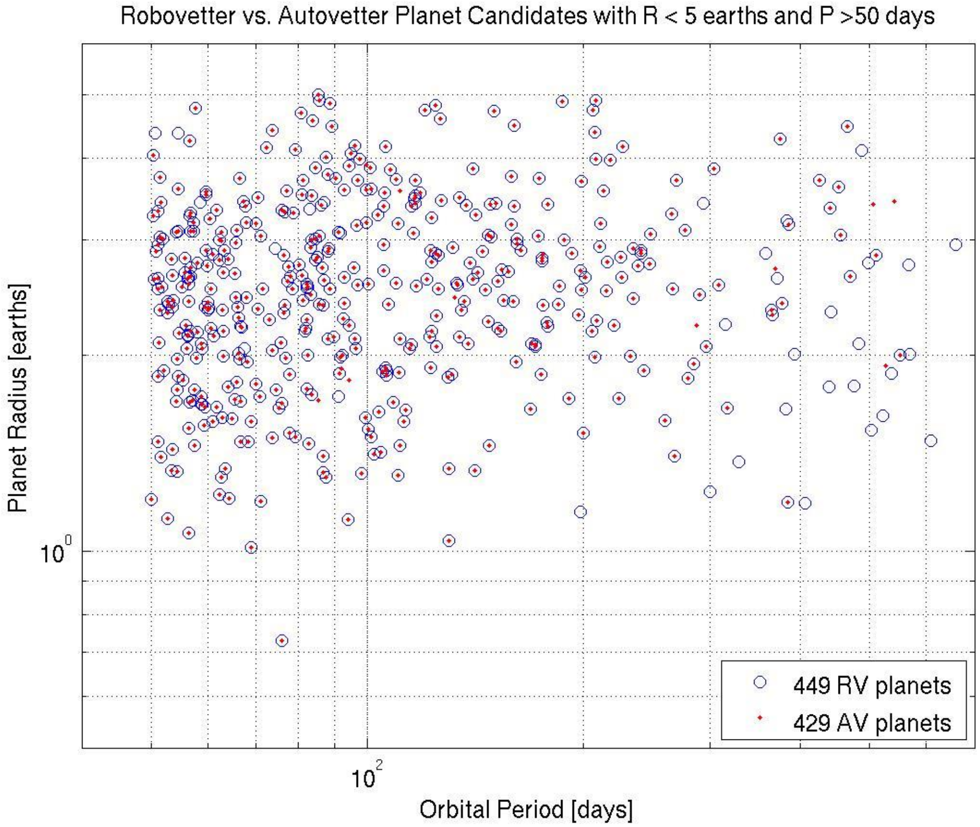

Figure 8. Robovetter vs. autovetter planet candidates in a regime that affects planetary occurrence rates. The robovetter has more candidates in the small radius and long period region of phase space.

For each TCE, the autovetter provides a posterior probability that it is a member of the class of PCs, which can be understood as a measure of the confidence, or reliability of the classification. Figure 9 shows the PC posterior probabilities of the autovetter and robovetter candidates from Figure 8. We expect that PCs in the low-SNR regime toward long periods and smaller radii would tend to have smaller PC posterior probabilities than other PCs; it is evident from Figure 9 that this is indeed the case.

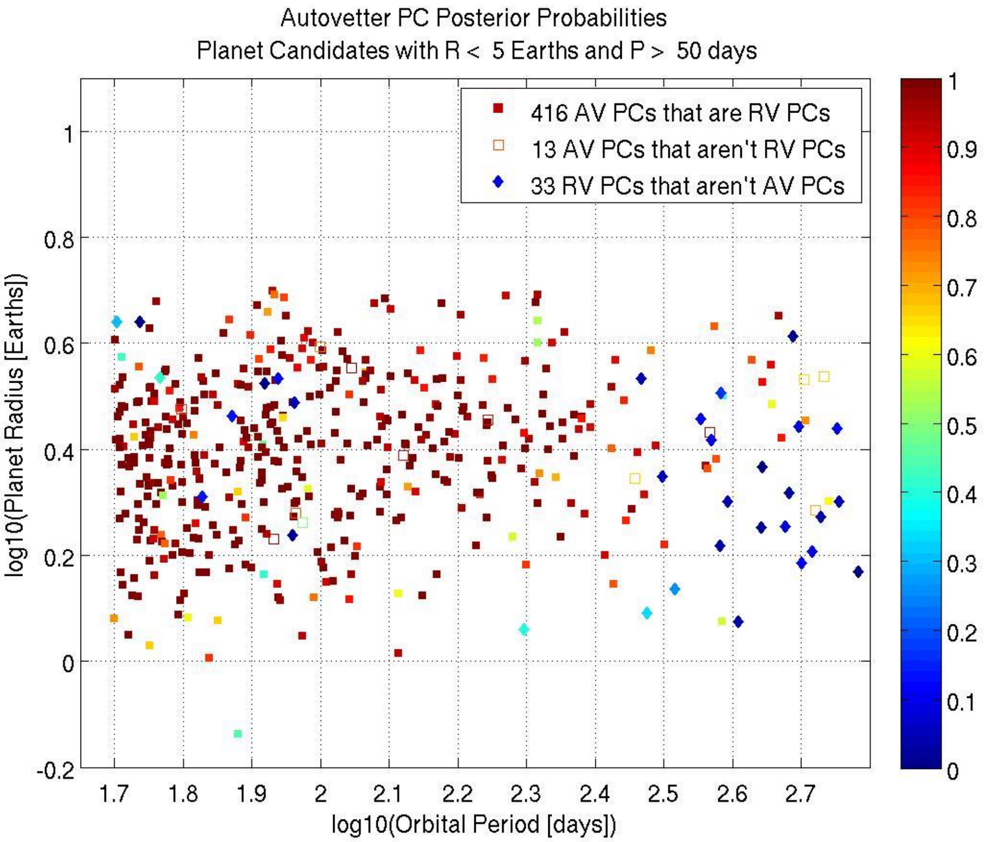

Figure 9. PC posterior probabilities for autovetter and robovetter planet candidates smaller than 5 R_{Earth} and with orbit periods longer than 50 days. Within this range there are 449 robovetter PCs and 429 autovetter PCs. In the plot, the 416 PCs common to both robovetter and autovetter are represented by filled squares, the 13 autovetter PCs that are not robovetter PCs are represented by empty squares, and the 33 robovetter PCs that are not autovetter PCs are represented by filled diamonds. Among autovetter PCs (squares), the probabilities tend to be smaller for planets toward the long period, small radius regime, indicating that these candidates are in general less reliable than the others. The non-autovetter PCs have very small autovetter PC posterior probabilities (filled diamonds).

8.3.3 Analysis of Robovetter Flags

The robovetter provides four flags that appear in the NExScI KOI activity tables:

a) The ***Not Transit Like flag*** (NT) is set for TCEs whose light curves lack a transit signature characteristic of a planet or detached eclipsing binary. This includes TCEs with periodic light curve variations due to contact binaries, tidal binaries, starspots, and pulsations, as well as noise artifacts.
b) The ***Significant Secondary flag*** (SS) indicates TCEs whose light curves have a smaller 'dip' in the light curve that is characteristic of a secondary transit – a self-luminous star (or planet) being occulted by the primary.
c) The ***Centroid Offset flag*** (CO) indicates TCEs whose in-transit centroid differs from the out-of-transit centroid. This indicates that the transit signal originates from a star other than the target star, such as a background eclipsing binary.
d) The ***Ephemeris Match flag*** (EM) is set if the TCE's period and epoch were matched to the ephemeris of another TCE, indicating that the putative transit signal is an artifact induced by contamination.

TCEs whose light curves are periodic but not transit-like (such as sinusoidal variations) tend to have the Not Transit Like flag (a) set, but the autovetter tends to classify them as AFP. TCEs with flags (b) and (c) set will generally be classified as AFP by the autovetter. For TCEs with flag (d) set, all but the ones contaminated with RR Lyrae or the 459-day systematic would tend to be classified as AFP by the autovetter (see discussion in section 6).

Table 6 breaks out the autovetter classifications for TCEs with each of the robovetter flags. The autovetter very rarely classifies TCEs with any of these flags as PCs. The autovetter shows excellent agreement with the robovetter SS flag, classifying TCEs with the SS flag as AFPs 96.8% of the time.

Table 6. Autovetter Classification of TCEs with Robovetter Flags

	Autovetter PC	Autovetter AFP	Autovetter NTP
CO flag (2177)	42 (1.9%)	1866 (85.7%)	269 (12.4%)
SS flag (3131)	42 (1.3%)	3032 (96.8%)	57 (1.8%)
EM flag (1910)	10 (0.5%)	1336 (70.0%)	564 (29.5%)
NT flag (13258)	45 (0.3%)	7197 (54.3%)	6016 (45.4%)

8.4 Summary: Comparison of the Autovetter and Robovetter in Practice

The autovetter and robovetter have followed two distinct approaches to arrive at the same goal – automation of the process of human classification of planet candidates to achieve robust and consistent vetting of the entire population of TCEs. The robovetter is an ***expert system*** that applies a set of explicit rules involving values of a focused set of attributes to arrive at a classification decision. The rules are tuned and iterated by knowledgeable experts to approximate a human decision, based on many individual cases. The autovetter is a ***supervised machine learning classifier*** that derives an implicit mapping between the values of a much broader set of attributes and a classification decision. The learning is supervised because it relies on a training set of representative

TCEs with labels (classifications) that are largely derived from humans and which we are reasonably confident are true.

There are two chief differences between the resulting catalogs: the autovetter provides an associated measure of confidence (posterior class probability) with each classification (which the robovetter does not), and the robovetter provides a specific reason for each classification (which the autovetter does not).

The posterior class probabilities ultimately derive from the relative votes of the random forest for each class. Visualizing the votes on a ternary diagram can qualitatively indicate the degree of confidence we should have in a classification by revealing whether a particular TCE is well within a decision region or close to a corner (high confidence), or is close to a decision boundary (lower confidence). The degree of confidence is quantified in the form of a posterior probability that the TCE is a member of each of the three classes. Posterior probabilities can be advantageously used in statistical studies such as occurrence rate calculations to de-weight planet candidates that are at the noisy edges of the planet catalog.

While the autovetter and robovetter agree on the classification of the vast majority of PCs, they do not agree in every case. For example the autovetter tends to classify planets that are large enough and bright enough to have secondary eclipses as AFPs, while the robovetter is tuned to be able to identify them.

Another important difference is that while the autovetter has three classifications, PC/AFP/NTP, the robovetter has four flags: Not Transit-Like, Significant Secondary, Centroid Offset, and Ephemeris Match. These flags allow various sub-populations (e.g., on- and off-target EBs, off-target flux PCs, secondary eclipses) to be selected for further study.

9. References

[Batalha 2013] Batalha, N.M. et al. “Planetary Candidates Observed by Kepler III. Analysis of the First 16 Months of Data”, 2013 ApJS, 204, 24

[Borucki 2011a] Borucki, W.J. et al. “Characteristics of Planetary Candidates Based on the First Data Set”, 2011 ApJ, 728, 117

[Borucki 2011b] Borucki, W.J. et al. “Characteristics of Planetary Candidates Observed by Kepler II. Analysis of the First Four Months of Data”, 2011 ApJ, 736, 19

[Breiman 2001] Breiman, L. “Random Forests”, 2001 Machine Learning, 45

[Burke 2014] Burke, C.J. et al. “Planetary Candidates Observed by Kepler IV. Planet Sample from Q1-Q8 (22 months)”, 2014 ApJS, 210, 19

[Burke 2015] Burke, C.J. et al. “Terrestrial Planet Occurrence Rates for the Kepler GK Dwarf Sample”, 2015 ApJ, accepted; arXiv:1506.04175

[Coughlin 2014] Coughlin, J. et al. “Contamination in the Kepler Field. Identification of 685 KOIs as false positives via ephemeris-matching based on Q1-Q12 data”, 2014 ApJ 147, 119

[Coughlin 2015] Coughlin, J. et al., “Planetary Candidates Observed by Kepler. VII. The First Fully Automated Catalog Based on the Entire 48 Month Dataset (Q1-Q17 DR24)”, 2015 ApJ, in preparation.

[James 2013] James, G. et al. *An Introduction to Statistical Learning*, Springer 2013

[Jenkins 2010a] Jenkins, J. M., Caldwell, D. A., Chandrasekaran, H., et al. 2010, ApJ, 713, L87

[Jenkins 2010b] Jenkins, J. M., Chandrasekaran, H., McCauliff, S. D., et al. 2010b, in Society of Photo-Optical Instrumentation Engineers (SPIE) Conference Series, Vol. 7740

[Jenkins 2015a] Jenkins, J.M., Seader, S.E. and Burke, C.J., “Planet Detection Metrics: Statistical Bootstrap Test”, 2015, KSCI-19086-001

[Jenkins 2015b] Jenkins, J.M. et al. “Discovery and validation of Kepler-7016b: A 1.6 R_{Earth} Super Earth Exoplanet in the Habitable Zone of a G2 Star”, 2015 ApJ, accepted.

[Jenkins 2015c] Jenkins, J.M. et al. “Automatic Classification of Kepler Threshold Crossing Events: 363 New likely Kepler planetary candidates identified in the first 46 months”, 2015 ApJ, in preparation.

[McCauliff 2015] McCauliff, S. D. et al. “Automatic Classification of Kepler Planetary Transit Candidates”, 2015 ApJ 806, 6

[Mullally 2015] Mullally, F. et al. “Planetary Candidates Observed by Kepler VI. Planet Sample from Q1-Q16 (47 Months)”, 2015 ApJS, 217, 31

[Rowe 2015] Rowe, J.F. et al. “Planetary Candidates Observed by Kepler V. Planet Sample from Q1-Q12 (36 Months)”, 2015 ApJS, 217, 16

[Seader 2015] Seader, S.E. et al. “Detection of Potential Transit Signals in 17 Quarters of Kepler Mission Data”, 2015 ApJS, 217, 18

[Thompson 2015] Thompson S. et al. “A Machine Learning Technique to Identify Transit Shaped Signals”, 2015 ApJ, submitted.

[Wu 2010] Wu, H., Twicken, J. D., Tenenbaum, P., et al. 2010, in Society of Photo-Optical Instrumentation Engineers (SPIE) Conference Series, Vol. 7740, Society of Photo-Optical Instrumentation Engineers (SPIE) Conference Series, 19